processes

MDPI

Article

NMR Analysis of Imbibition and Damage Mechanisms of Fracturing Fluid in Jimsar Shale Oil Reservoirs

Lei Bai [1,2,3], Huiying Guo [2,3], Zhaowen Jiang [2,3], Yating Sun [2,3], Yan Li [2,3], Yuning Han [1], Xuejing Han [1], Shenglai Yang [1,*] and Shuai Zhao [1,*]

[1] College of Petroleum Engineering, China University of Petroleum (Beijing), Beijing 102249, China
[2] Xinjiang Oilfield Company, Petro China, Karamay 834000, China
[3] Xinjiang Laboratory of Shale Oil Exploration and Development, Karamay 834000, China
* Correspondence: yangsl@cup.edu.cn (S.Y.); shuaizhao0726@163.com (S.Z.)

Abstract

Optimizing the shut-in and flowback processes is crucial for improving oil recovery and mitigating formation damage in shale oil development. However, the mechanisms governing fracturing fluid migration and its impact on permeability, particularly across different lithologies, remain poorly understood. This study investigates the spontaneous imbibition behavior of fracturing fluid and the resulting permeability damage in two predominant lithotypes (dolomitic siltstone and argillaceous siltstone) from the Jimsar shale oil reservoir. By integrating low-field nuclear magnetic resonance (NMR) monitoring with core flooding experiments, we dynamically characterize fluid migration and quantitatively evaluate damage rates. The results reveal that lithology exerts a fundamental control on these processes. Dolomitic siltstone, with its higher brittle mineral content and well-connected pore network, facilitates deeper fracturing fluid invasion (30.47 mm) and more efficient oil displacement. In contrast, argillaceous siltstone, which is rich in clay minerals, exhibits stronger capillary trapping and suffers more severe permeability damage (~70%) compared to dolomitic siltstone (~46%), primarily due to the synergistic effects of water blocking and clay swelling. Furthermore, the impact of shut-in time on permeability damage follows a non-monotonic trend, reflecting a dynamic competition between imbibition-driven oil recovery and fluid-induced damage. Flowback analysis on core plugs reveals an economic critical point, beyond which further permeability recovery becomes marginal. This core-scale finding underscores the importance of the initial flowback stage for efficient cleanup and provides a scientific basis for optimizing flowback strategies in the Jimsar shale and similar unconventional reservoirs. These findings offer guidance for designing lithology-specific fracturing fluid systems, optimizing shut-in durations, and tailoring flowback strategies in the Jimsar shale and analogous unconventional reservoirs.

Keywords: fracturing fluid imbibition; permeability damage; nuclear magnetic resonance (NMR); flowback optimization

check for updates

Academic Editor: Tao Zhang

Received: 31 October 2025
Revised: 21 November 2025
Accepted: 28 November 2025
Published: 1 December 2025

Citation: Bai, L.; Guo, H.; Jiang, Z.; Sun, Y.; Li, Y.; Han, Y.; Han, X.; Yang, S.; Zhao, S. NMR Analysis of Imbibition and Damage Mechanisms of Fracturing Fluid in Jimsar Shale Oil Reservoirs. *Processes* **2025**, *13*, 3875. https://doi.org/10.3390/pr13123875

Copyright: © 2025 by the authors. Licensee MDPI, Basel, Switzerland. This article is an open access article distributed under the terms and conditions of the Creative Commons Attribution (CC BY) license (https://creativecommons.org/licenses/by/4.0/).

1. Introduction

With the continuous decline in global conventional hydrocarbon production and increasing energy demand, unconventional resources have emerged as an increasingly viable alternative, facilitated by a series of technological breakthroughs [1,2]. The rapid development of shale oil and gas in recent years has garnered significant attention, establishing these resources as a focal point in petroleum exploration and development research [3].

Shale reservoirs are typically characterized by ultra-low porosity and permeability, necessitating effective stimulation techniques, such as horizontal drilling and massive hydraulic fracturing, for economic development [4,5]. These technologies create extensive fracture networks within the reservoir, which significantly increase the contact area for hydrocarbon flow and lead to high initial production rates [6].

During hydraulic fracturing, large volumes of fluid are injected into the formation to propagate these fractures. A substantial portion of this fluid, however, invades the shale matrix under high pressure differentials. In subsequent flowback and production phases, as reservoir energy depletes, the invaded fluid can cause significant formation damage through various mechanisms, including aqueous phase trapping (water blocking), clay swelling, and fine migration. These mechanisms ultimately impair permeability and reduce the effectiveness of the stimulation treatment [7–9]. It is noteworthy that the key parameters controlling these aqueous fracturing fluid interactions (e.g., imbibition and damage control) differ fundamentally from those in gas-based enhanced oil recovery (EOR) processes, where the minimum miscibility pressure (MMP) is paramount [10]. Field experience and experimental studies have suggested that implementing a controlled shut-in period (soaking) after fracturing but before flowback may help mitigate such damage and potentially enhance oil recovery through spontaneous imbibition. In this process, the fracturing fluid displaces oil from the matrix pores into the fractures under capillary forces [11,12].

Despite these observations, the fundamental mechanisms governing fracturing fluid migration and oil exchange within shale's complex pore systems during shut-in remain poorly understood. This knowledge gap fuels ongoing debate and results in a lack of scientific basis for optimizing shut-in duration and flowback strategy. The role of reservoir lithology, a primary factor controlling pore structure and rock-fluid interactions, is particularly unclear. Moreover, the dynamic competition between the positive effect of oil displacement via imbibition and the negative effect of permeability damage due to fluid retention has not been quantitatively resolved.

Previous studies utilizing low-field nuclear magnetic resonance (NMR) have demonstrated its capability for non-destructively monitoring fluid distribution and pore-scale occupancy changes in real time [13–15]. However, many of these investigations were conducted under ambient conditions or focused primarily on imbibition dynamics without direct, concurrent evaluation of the resulting permeability damage under simulated reservoir conditions. Furthermore, a systematic evaluation that links the spatiotemporal fluid migration patterns revealed by NMR with the resulting permeability damage—while considering the critical interplay between lithology, shut-in time, and flowback volume—is often lacking.

To address these nuanced gaps, this study introduces a novel and comprehensive approach by synergistically combining NMR-monitored spontaneous imbibition experiments with core flooding tests for permeability damage evaluation, all conducted under simulated in situ conditions for the Jimsar shale oil reservoir. We target two predominant lithotypes: dolomitic siltstone and argillaceous siltstone. Beyond conventional NMR T_2 spectral analysis, we uniquely employ one-dimensional (1D) profiling to dynamically track the frontal advancement of the fracturing fluid, providing a spatially-resolved understanding of the imbibition process. The primary objectives are: (1) To dynamically characterize the spatiotemporal migration patterns of fracturing fluid and its oil displacement efficiency in different lithologies using NMR T_2 spectra and 1D profiling; (2) To quantify the permeability damage rate (η_o) and identify the dominant damage mechanisms for each lithology; (3) To investigate the competing effects of shut-in time and the efficiency of different flowback volumes in mitigating damage. The findings from this work are expected to provide a

mechanistic understanding and a practical scientific basis for optimizing fracturing fluid systems, shut-in schedules, and flowback strategies in the Jimsar shale oil reservoir and similar unconventional plays.

2. Experimental Materials and Methods

2.1. Materials

The experimental fluids comprised a slickwater fracturing fluid (XC-4, provided by Xinjiang Oilfield Company, Karamay, China) used in the Jimsar field and simulated oil. The simulated oil was prepared by mixing dehydrated and degassed crude oil from the same field with neutral kerosene at a mass ratio of 3:7. All shale core plugs were drilled from full-diameter cores retrieved from the Jimsar shale oil reservoir and were machined to a standard size of approximately 2.5 cm in diameter and 7.0 cm in length. Fragments damaged during the coring process were reserved for mineralogical analysis. The sampled rocks represent two typical lithological types in this block: dolomitic siltstone and argillaceous siltstone. To isolate and highlight the fundamental control of lithology on the processes under investigation, core selection for both lithotypes was carefully conducted to achieve comparable initial porosity and permeability ranges (Table 1). This controlled approach ensures that observed differences in fluid migration and damage can be confidently attributed to lithological factors (mineral composition and microstructure) rather than to initial petrophysical variations.

Table 1. Petrophysical property parameters of the samples.

Label	D/cm	L/cm	φ/%	k/md	Lithology
JH-1	2.53	7.12	14.21	0.18	Dolomitic siltstone
JH-2	2.51	7.04	13.22	0.17	Dolomitic siltstone
JH-3	2.52	7.16	15.14	0.15	Dolomitic siltstone
JH-4	2.57	7.08	12.89	0.11	Dolomitic siltstone
JH-5	2.57	7.11	14.11	0.12	Dolomitic siltstone
JH-6	2.49	7.14	12.68	0.14	Dolomitic siltstone
JH-7	2.47	7.12	15.23	0.13	Dolomitic siltstone
JH-8	2.49	7.06	12.94	0.12	Dolomitic siltstone
JH-9	2.51	7.11	13.52	0.14	Dolomitic siltstone
JH-10	2.53	7.14	14.16	0.11	Argillaceous siltstone
JH-11	2.24	7.12	13.95	0.13	Argillaceous siltstone
JH-12	2.52	7.10	12.55	0.15	Argillaceous siltstone
JH-13	2.53	7.11	14.18	0.17	Argillaceous siltstone
JH-14	2.51	7.06	13.35	0.12	Argillaceous siltstone
JH-15	2.54	7.04	14.12	0.14	Argillaceous siltstone
JH-16	2.52	7.12	12.85	0.13	Argillaceous siltstone
JH-17	2.57	7.09	13.70	0.14	Argillaceous siltstone
JH-18	2.51	7.12	12.69	0.12	Argillaceous siltstone

Prior to the experiments, the cores were cleaned using a mixture of 75% alcohol and 25% benzene to remove residual oil and then dried. Basic petrophysical properties, including helium porosity and permeability, were measured; the results are summarized in Table 1. A total of eighteen cores were used (nine for each lithotype), and the reported results for each lithology are derived from this sample set. To preserve pore structure integrity and avoid compounding damage, each core was used for only a single experiment—either for NMR imbibition monitoring or for a specific permeability damage evaluation under unique conditions (e.g., a specific shut-in time or flowback volume). The two lithotypes exhibit similar porosity and permeability ranges but differ significantly in their mineralogical composition.

2.2. Petrological Analysis Experiments

Quantitative analysis of the rock sample mineral composition was performed using a DX-2700 X-ray diffractometer (Dandong Tongda Science and Technology Co., Ltd., Dandong, China). Casting thin section (CTS) analysis involved injecting colored epoxy resin into the rock pores under vacuum. The rock was then ground into thin sections and examined under a microscope to observe the reservoir microstructure. Microstructural observations were conducted using a Quanta 200F field emission scanning electron microscope (SEM, FEI Company, Hillsboro, OR, USA). Freshly broken rock surfaces were irradiated with an electron beam to directly observe interstitial materials, pore structures, and cementation characteristics.

2.3. Spontaneous Imbibition Experiments Using NMR

To quantitatively investigate the spontaneous imbibition and migration characteristics of fracturing fluid from fractures into the matrix, all surfaces of the experimental core samples were sealed with polytetrafluoroethylene (PTFE), leaving only one end face exposed to simulate a fracture surface. A schematic of the treated core is shown in Figure 1. PTFE, being a non-paramagnetic material, introduces negligible interference with the magnetic field. Preliminary tests confirmed that the PTFE seal did not introduce any measurable interference or distortion in the NMR signals [16]. The experiments were conducted using a SPEC-210 low-field nuclear magnetic resonance analyzer (Beijing SPEC Technology Development Co., Ltd., Beijing, China). This instrument can acquire NMR signals from the entire core or specific cross-sections, which can be converted into T_2 relaxation time distributions and 1D NMR profiles. The key parameters for the NMR experiments are summarized in Table 2.

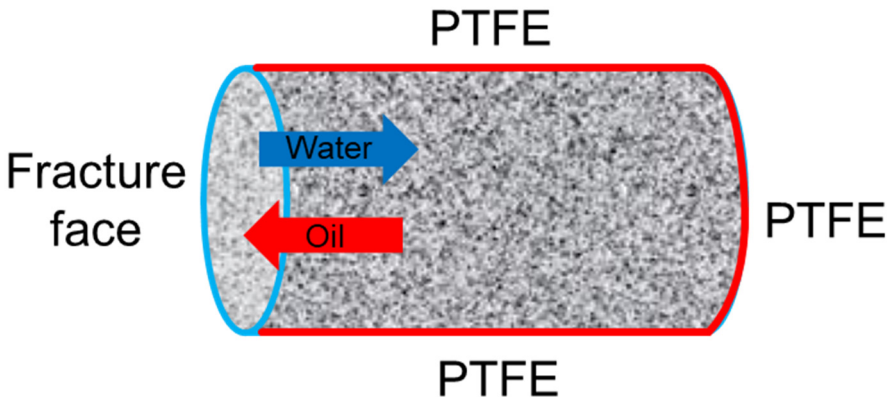

Figure 1. Schematic of experimental core in imbibition.

Table 2. Key parameters of the NMR experiments.

Function	Pulse Sequences	SF (MHz)	DW (us)	TAU (us)	TE (ms)	SCAN
T_2	CPMG	14.06	2.0	150	0.3	64
1D frequency	GR-HSE	14.06	2.0	150	1.45	128

2.4. Permeability Damage Evaluation Experiment

The permeability damage evaluation was conducted using a core flooding system (TC-180) developed in-house. The apparatus primarily consists of a constant-temperature oven, temperature and pressure sensors, a high-temperature and high-pressure core holder, confining pressure pumps, flow pressure pumps, a back-pressure pump, and a data acquisition system, as illustrated in Figure 2. The core holder employs a special sleeve to ensure overall system sealing under high-temperature and high-pressure conditions, with maximum

working pressures and temperatures of 180 MPa and 150 °C, respectively. The core samples were tightly sealed within a rubber sleeve in the core holder, and confining pressure was applied to simulate the overburden stress. The flow was unidirectional: fracturing fluid was injected from one end, and oil was injected from the opposite end during flowback, mimicking the field scenario where fluid enters from the fracture face and is produced back through the same network. The experimental temperature was set at 80 °C to simulate the reservoir condition. The initial pore pressure was set to 50 MPa, representing the original formation pressure, and the confining pressure was maintained at 80 MPa to simulate the overburden rock pressure. The pressure differential across the core during the flowback phase was controlled at approximately 10–20 MPa, corresponding to the typical drawdown pressure observed in the Jimsar shale oil field during early production stages. This range is consistent with field data from nearby wells, where bottom-hole flowing pressure drops of 10–25 MPa have been recorded during the initial flowback period after hydraulic fracturing. Therefore, the selected pressure differential is representative of the near-wellbore region under actual production conditions, where most fluid-induced permeability damage is expected to occur.

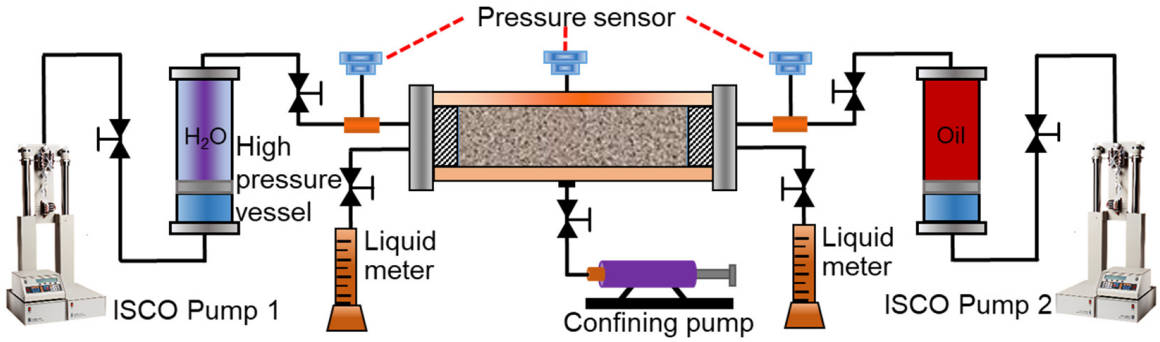

Figure 2. Schematic diagram of the experimental setup for permeability damage evaluation.

The experimental procedure was as follows:

(1) The cleaned and dried core was placed under vacuum for 24 h and then saturated with simulated oil for another 24 h. The mass of the oil-saturated core was measured.

(2) The oil-saturated core was placed into the core holder. As shown in Figure 2, the left-side pipeline and intermediate container were filled with fracturing fluid, while the right-side pipeline and intermediate container were filled with simulated oil.

(3) The confining pressure pump was activated until the pressure reached the set value. ISCO Pump 2 was then opened to inject oil into the core from the opposite direction. After the flow stabilized, the initial oil permeability (k_{o1}) was measured.

(4) ISCO Pump 1 was opened to inject 1 PV of fracturing fluid into the core from the forward direction. Subsequently, the valves at both ends of the core holder were closed to simulate the shut-in process.

(5) ISCO Pump 2 was opened again to inject simulated oil into the core from the opposite direction. When the produced fluid volume reached the set value, the oil permeability (k_{o2}) was measured again.

(6) The permeability damage rate (η_o) was calculated using the following formula based on k_{o1} and k_{o2}:

$$\eta_o = \frac{k_{o1} - k_{o2}}{k_{o1}} \times 100\%$$

3. Results and Discussion

3.1. Mineral Composition and Microstructure of the Reservoir

Mineral composition analysis of the drilled core samples was conducted using a DX-2700 X-ray diffractometer; the results are presented in Table 3. The analysis shows that the Jimsar shale reservoir is composed primarily of quartz, feldspar (K-feldspar and plagioclase), carbonate minerals (calcite, dolomite, and ankerite), and clay minerals. Overall, the high brittle mineral content provides a material basis for forming complex fracture networks.

Table 3. Distribution of Mineral Composition of Shale of Jimsar Shale.

Label	Clay	Qtz	Kfs	Pl	Cal	Dol	Ank
JH-1	6.3	17.8	—	23.9	6.6	—	45.4
JH-2	4.1	12.9	13.4	14.8	8.6	46.2	—
JH-3	7.5	21.2	—	33.7	—	—	37.6
JH-4	5.8	23.1	20.6	38.3	—	—	12.2
JH-5	6.2	18.4	23.7	30.9	8.9	—	11.9
JH-6	4.3	23.9	—	46.8	11.9	—	13.1
JH-7	5.2	28.9	—	41.3	—	13.1	11.5
JH-8	6.1	19.8	9.9	28.8	19.6	—	15.8
JH-9	4.3	21.5	—	36.8	8.8	—	28.6
JH-10	19.4	13.4	6.5	23.4	4.8	32.5	—
JH-11	18.1	12.8	8.1	24.4	7.1	11.2	18.3
JH-12	16.9	19.4	9.9	29.7	12.8	—	11.3
JH-13	17.8	21.0	13.8	29.5	12.3	5.6	—
JH-14	14.9	23.3	12.0	31.2	11.2	7.4	—
JH-15	18.2	20.4	9.2	21.7	10.6	6.8	13.1
JH-16	19.8	17.9	21.2	15.8	17.1	—	8.2
JH-17	16.5	14.7	23.8	30.2	4.1	—	10.7
JH-18	19.3	20.4	14.8	28.5	7.8	—	9.2

The mineral compositions of the two lithotypes differ significantly, which fundamentally influences their distinct imbibition and damage behaviors. Dolomitic siltstone (samples JH-1 to JH-9) is rich in carbonate minerals (mainly dolomite and ankerite), with generally high contents (exceeding 45% in some samples) and a low clay mineral content (average 6.0%). In contrast, argillaceous siltstone (samples JH-10 to JH-18) exhibits a significantly higher clay mineral content (average 17.5%) and a relatively lower carbonate mineral content. Rigid minerals, such as quartz and feldspar, account for a considerable proportion in both lithotypes; however, the feldspar content (especially plagioclase) is generally higher in dolomitic siltstone.

The results of casting thin section (CTS) and scanning electron microscopy (SEM) analyses, presented in Figure 3 (partially reproduced from Figure 5 of ref. [17], with permission from Processes), further reveal the microstructural differences between the two lithotypes. The Jimsar shale contains various pore types, including intergranular, intercrystalline, and dissolution pores. The CTS image of argillaceous siltstone (Figure 3A) indicates that the intergranular spaces are primarily filled with clay minerals, with predominantly basal cementation resulting in a denser microstructure. SEM observations (Figure 3C) reveal the presence of illite/smectite mixed-layer minerals. These flaky and flocculent clay minerals form numerous complex micropores but are also prone to swelling upon water contact, potentially damaging flow pathways. In contrast, the CTS image of dolomitic siltstone (Figure 3B) shows that it consists mainly of detrital grains with point or line contacts between particles, and the cementation is primarily of the pore-filling or concave-convex type. This structure is relatively loose, with more developed pores. SEM images (Figure 3D)

show well-developed intergranular pores, with euhedral rhombohedral ankerite crystals visible within the pores. This predominantly grain-supported framework, characterized by high rigid mineral content and a relatively open pore system, provides better storage space and fluid migration pathways.

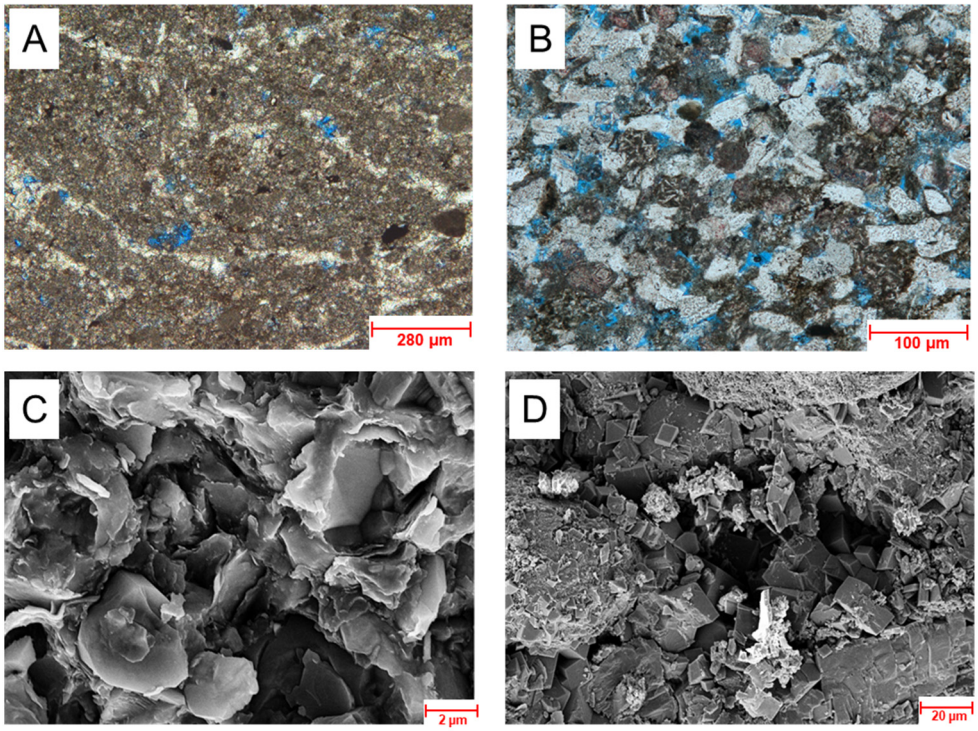

Figure 3. Comparative analysis of CTS and SEM images of different lithological shale. Parts of this figure are reproduced from Figure 5 of ref. [17] to establish the context of the shared core sample, while this study focuses on a distinct research objective. (**A**) CTS images of argillaceous shale. (**B**) CTS image of dolomitic siltstone. (**C**) SEM image of argillaceous shale, showing the presence of illite/smectite mixed-layer minerals. (**D**) SEM images of dolomitic siltstone with developed intergranular pores visible.

3.2. Fracturing Fluid Imbibition Characteristics

During the middle and late stages of fracturing and production, formation energy depletes rapidly, causing the pressure difference between fractures and the matrix to gradually equilibrate. Under these conditions, spontaneous imbibition occurs via capillary forces, displacing oil from the matrix pores into the fractures, thereby enabling oil production. To reveal the microscopic mechanisms of spontaneous imbibition and oil displacement within the shale matrix, this study selected core samples of two typical lithotypes (dolomitic siltstone and argillaceous siltstone) from the Jimsar area. Systematic spontaneous imbibition experiments were conducted, and the entire process was monitored precisely using NMR technology.

3.2.1. Characteristics of Fracturing Fluid Invasion into Cores

The 1D NMR scanning results during spontaneous imbibition for the two lithotypes are presented in Figures 4 and 5. The NMR signal intensity reflects the oil saturation at various locations within the core; a stronger signal corresponds to a higher oil content. In the initial state (before imbibition began), the NMR signal intensity curves along the core axes were relatively flat, indicating high initial oil saturation and good pore connectivity. A further comparison shows that the overall signal intensity of the dolomitic siltstone core (Figure 4) is significantly higher than that of the argillaceous siltstone core (Figure 5),

preliminarily suggesting that dolomitic siltstone possesses superior storage capacity, likely due to more developed and better-connected pore spaces.

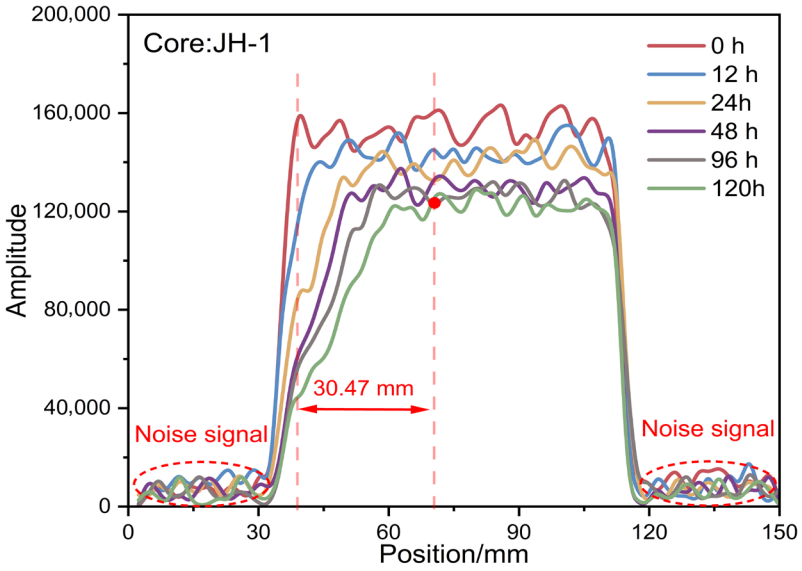

Figure 4. One-dimensional NMR scanning curves during the imbibition process for the dolomitic siltstone core.

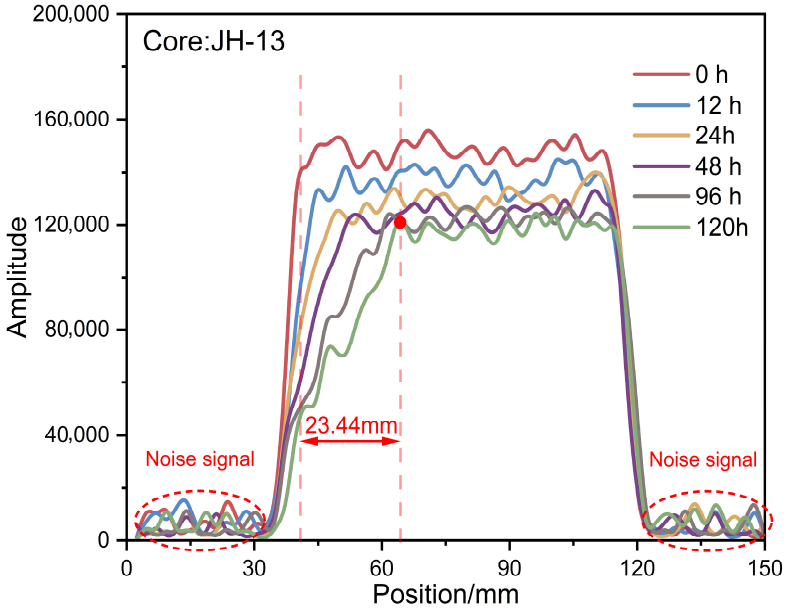

Figure 5. One-dimensional NMR scanning curves during the imbibition process for the argillaceous siltstone core.

As spontaneous imbibition proceeds, the NMR signal intensity decreases gradually from the imbibition face inward, indicating that the fracturing fluid primarily invades the near-end regions and struggles to reach the deeper parts of the core. Specifically, during the early imbibition stage (0–24 h), the signal intensity near the imbibition face decreases rapidly. As time extends to 24–120 h, the signal decay rate slows significantly, reflecting the rapid attenuation of the imbibition drive with increasing distance and time.

To quantitatively characterize the invasion range, the point where the NMR signal curves at 96 h and 120 h of imbibition first intersect is defined as the maximum invasion front. Based on this, the final invasion depth of the fracturing fluid is measured to be 30.47 mm in the dolomitic siltstone core, compared to only 23.44 mm in the argillaceous

siltstone core. This significant difference in invasion depth is primarily controlled by the distinct pore structures of the two lithotypes and their constraining mechanisms on the imbibition drive. The higher initial oil content in dolomitic siltstone implies a more developed pore structure, relatively larger throats, and better connectivity, providing preferential pathways for fracturing fluid flow and significantly reducing flow resistance. In contrast, the high clay mineral content in argillaceous siltstone tends to form more developed micro-pore systems and highly tortuous flow paths. This not only increases the capillary resistance to fluid flow but also makes the flow channels more susceptible to physical blockage effects (such as the Jamin effect and fine migration) during the middle and late stages of imbibition, leading to rapid depletion of the imbibition drive and severely restricting the final invasion depth. The more efficient invasion in dolomitic siltstone suggests a pore network with more continuous and favorable pathways for capillary imbibition, whereas the constrained invasion in argillaceous siltstone reflects the dominant role of strong capillary trapping in a more heterogeneous and fractal pore system, as capillary-driven flow is significantly influenced by the fractal characteristics of the dynamic fluid pathways [18]. This direct visualization of the spatially advancing invasion front, enabled by 1D NMR profiling, provides a critical dimension of analysis that complements the pore-scale information derived from the T_2 relaxation spectra.

3.2.2. Dynamic Imbibition Analysis Based on NMR T_2 Relaxation

The temporal evolution of the T_2 relaxation spectra provides a powerful means to evaluate the microscopic dynamics of fracturing fluid invasion into oil-bearing cores. The decrease in the spectral area directly corresponds to the displacement and production of oil by the fracturing fluid. As shown in Figures 6 and 7, the core samples of both lithotypes exhibit a typical bimodal T_2 distribution in the initial oil-saturated state, indicating a dual-scale pore system comprising micropores (left peak) and macropores or microfractures (right peak).

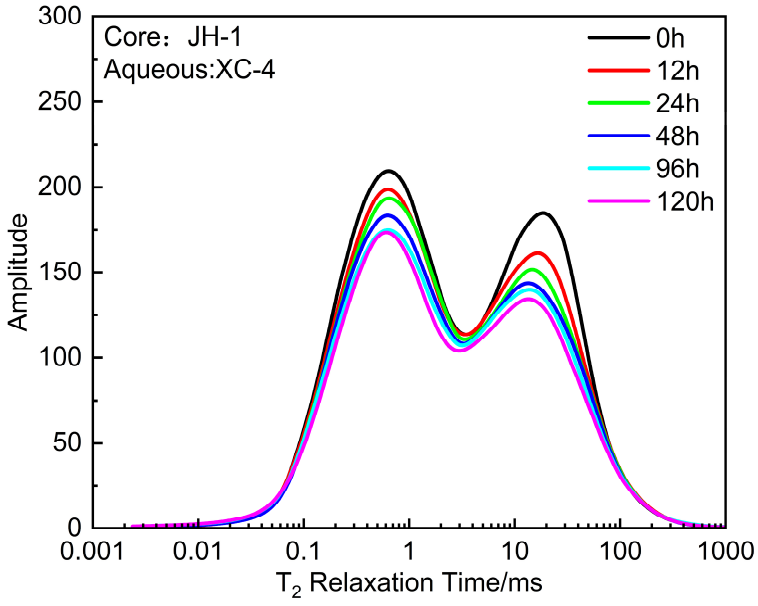

Figure 6. T_2 spectra during the imbibition process for the dolomitic siltstone core.

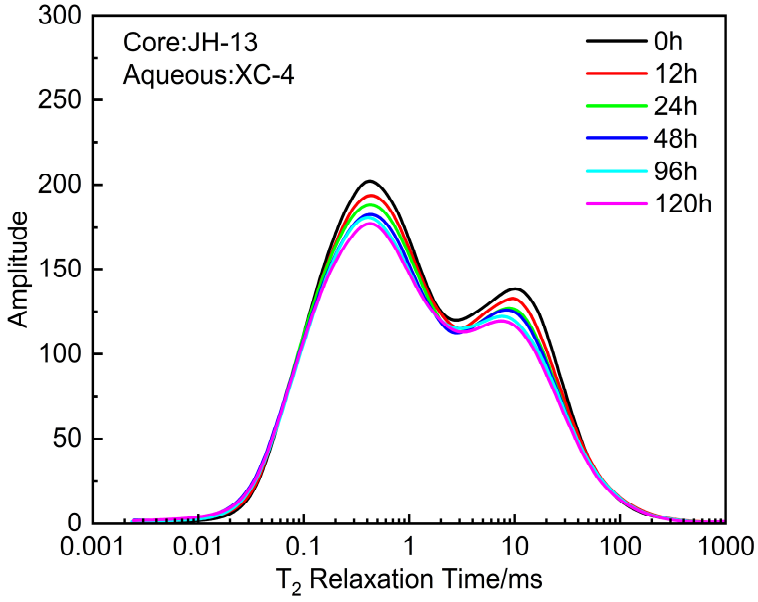

Figure 7. T_2 spectra during the imbibition process for the argillaceous siltstone core.

During the fracturing fluid imbibition process, the T_2 spectral areas of both cores show a continuous decreasing trend, visually reflecting the process of oil being displaced and produced. However, the signal attenuation characteristics in different pore ranges differ significantly between the two core types. For the dolomitic siltstone core (Figure 6), the signal intensity of the right peak (macropores/microfractures) decreases rapidly during the early imbibition stage (0–24 h), and the attenuation amplitude is significantly higher than that of the left peak. This indicates that the fracturing fluid preferentially enters larger pores and microfractures, efficiently displacing the oil within them. As imbibition proceeds, the attenuation of the right peak slows, while the signal of the left peak (micropores) begins to show a more pronounced decrease, suggesting that the fracturing fluid gradually propagates from the large pores into the adjacent network of smaller pores, demonstrating good displacement efficiency. This sequence reveals that in well-connected pore systems, the imbibition process follows a displacement path "from large to small, from main channels to branch pores". For the argillaceous siltstone core (Figure 7), the overall attenuation rate and amplitude of its T_2 spectrum are lower than those of the dolomitic siltstone. Although the right peak also attenuates preferentially, the rate of decrease is slower, and the left peak signal shows only a slight weakening throughout the entire process. This indicates that in argillaceous siltstone, not only is the invasion depth limited (as shown in Section 3.2.1), but the displacement efficiency for oil in various pore types is also generally lower. This is mainly attributed to the highly tortuous micro-pore system caused by the higher clay mineral content. Strong capillary trapping and the complex pore structure severely restrict the effective flow and displacement of the fracturing fluid, making it difficult to mobilize the oil effectively, especially the portion trapped in the micropores.

In summary, the differences in T_2 relaxation dynamics further confirm, at the pore scale, the controlling effect of lithology on imbibition behavior. Dolomitic siltstone, due to its developed macropore/fracture network and good pore connectivity, achieves effective mobilization of oil in both large and small pores. In contrast, argillaceous siltstone, due to strong capillary trapping and a tortuous micropore system, greatly limits the imbibition displacement efficiency of the fracturing fluid. This understanding is highly valuable for optimizing fracturing fluid formulations and shut-in strategies in unconventional reservoirs.

3.3. Degree of Permeability Damage Induced by Fracturing

While the fracturing fluid imbibes and displaces oil, its retention can also cause varying degrees of reservoir damage, leading to a decrease in matrix permeability and directly impacting subsequent production efficiency. This study systematically evaluated the effects of lithology, shut-in time, and flowback volume on the η_o through displacement experiments.

3.3.1. Influence of Lithology

Experimental results indicate that lithology is a key intrinsic factor controlling the degree of reservoir permeability damage. As shown in Table 4, under identical experimental conditions (72 h shut-in, 1.5 PV flowback), the η_o of argillaceous siltstone cores is as high as 70.1%, significantly higher than that of dolomitic siltstone (46.8%). This significant difference primarily stems from differences in mineral composition, pore structure, and the resulting damage mechanisms between the two lithotypes.

Table 4. Comparison of permeability damage rates (η_o) for cores of different lithologies.

Label	Lithology	k_{o1}/mD	k_{o2}/mD	η_o/%
JH-3	Dolomitic siltstone	0.079	0.042	46.8
JH-12	Argillaceous siltstone	0.068	0.020	70.1

The higher clay content in argillaceous siltstone makes it more susceptible to physico-chemical damage, a common concern in formation damage [19]. The utility of NMR in quantifying such formation damage, including fines invasion and its impact on permeability, has been demonstrated in previous studies. For example, Multi-Depth of Investigation (MDOI) NMR logs have been used to identify and quantify formation damage caused by mud fines invasion in near-wellbore regions [20]. Our core-scale findings, which reveal a lithology-dependent damage severity and mechanism (e.g., "water blocking + clay hydration swelling/fine migration" in argillaceous siltstone versus predominantly "water blocking" in dolomitic siltstone), thus contribute to a broader understanding of formation damage mechanisms that can be investigated using NMR techniques.

3.3.2. Influence of Shut-In Time

Shut-in time is a key operational parameter for balancing the benefits of imbibition displacement against the risks of reservoir damage. Experimental results (Figure 8) show that the η_o exhibits a complex non-monotonic relationship with shut-in time, with distinct response patterns for different lithologies. As the shut-in time increases from 24 to 120 h, the η_o for both core types initially increases and then decreases, but with notable lithological differences. For argillaceous siltstone, the damage rate peaks at 70.1% after 72 h of shut-in, representing a 27% increase compared to the 24 h value, and then slowly decreases to 63.3% at 120 h, remaining relatively high. In contrast, for dolomitic siltstone, the damage rate peaks earlier, at 48 h (46.8%), with a significantly lower peak magnitude, and shows a more pronounced decline thereafter, decreasing to 38.5% by 120 h.

This non-monotonic trend essentially results from the dynamic competition between the damage effects caused by fracturing fluid retention and the cleanup effects resulting from oil displacement over time and space. During the early shut-in stage, capillary forces continuously drive the spontaneous imbibition of fracturing fluid deeper into the core. At this stage, the volume and extent of fracturing fluid invasion keep expanding, fully activating the damage mechanisms. Specifically, the water block zone expands; fracturing fluid fills more micropores, forming extensive aqueous phase trapping; in argillaceous siltstone, clay minerals have more time to undergo hydration, swelling, and dispersion, with the plugging effect intensifying over time; simultaneously, as the oil-water contact area

increases, the negative impact of interfacial resistance on flow becomes more significant. During this phase, the amount of oil displaced by imbibition is relatively small and fails to form an effective flow network. Thus, the damage effect dominates absolutely, manifested as a continuous increase in the damage rate.

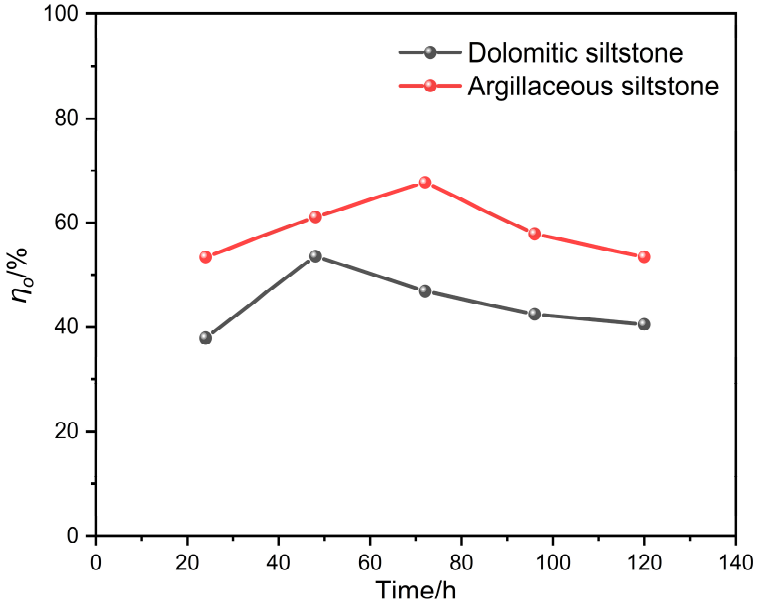

Figure 8. Permeability damage rate (η_o) versus shut-in time for Jimsar shale cores.

As the shut-in time extends further, the efficiency of imbibition displacement increases significantly, gradually manifesting the cleanup effect. Experimental data show that the imbibition displacement efficiency enters a rapid growth phase after 48 h, increasing from 38.7% to 58.9% at 120 h. The continuously displaced oil forms continuous oil filaments or banks within the pores, gradually connecting and establishing new oil flow pathways. Concurrently, part of the retained fracturing fluid is segmented and isolated by the reconnected oil phase, and its hindrance to oil flow is relatively reduced. In this stage, the positive cleanup effect generated by imbibition displacement begins to surpass the damage effect caused by fluid retention, macroscopically manifested as a slow decline in the damage rate.

This dynamic competition can be further elucidated through a semi-quantitative analysis integrating the permeability damage and NMR imbibition data. The peak in η_o observed between 48 and 72 h (Figure 8) coincides with the saturation of signal attenuation in the right peak (macropores/microfractures) of the NMR T_2 spectra (Figures 6 and 7). This correlation indicates that the early-stage dominance of damage mechanisms (e.g., water blocking and clay swelling) is subsequently counteracted by the increasing efficiency of spontaneous imbibition. The approximately 20% increase in oil displacement efficiency from 48 h to 120 h facilitates the reconnection of isolated oil phases and the establishment of new flow pathways, thereby partially offsetting the initial damage. The turning point in the permeability damage profile is, therefore, governed by the pore-throat structure of the specific lithology, which controls the relative rates of damage accumulation and imbibition recovery. Although the formulation of a dimensionless parameter falls beyond the scope of this study, this integrated analysis provides a robust experimental foundation for future development of such metrics, for instance, an Imbibition-to-Damage Ratio (IDR).

3.3.3. Influence of Flowback Volume

Flowback volume, as the most directly controllable parameter in field operations, directly determines the efficiency of removing retained fracturing fluid and is a key en-

gineering means for mitigating reservoir damage. Experimental results indicate that the η_o decreases exponentially with increasing flowback volume, but the improvement effect exhibits significant diminishing marginal returns (Figure 9). Specifically, when the flowback volume increases from 1.0 PV to 2.0 PV, the damage rate for dolomitic siltstone decreases significantly from 64.8% to 38.9%, and for argillaceous siltstone from 74.4% to 59.4%, representing reductions of 25.9 and 15.0 percentage points, respectively. However, when the flowback volume is further increased to 3.0 PV, the improvement in damage rate narrows sharply, with the damage rates for dolomitic and argillaceous siltstone decreasing by only 1.4 and 1.9 percentage points, respectively. This indicates that the efficiency of restoring permeability by merely increasing the flowback volume becomes very limited at this stage.

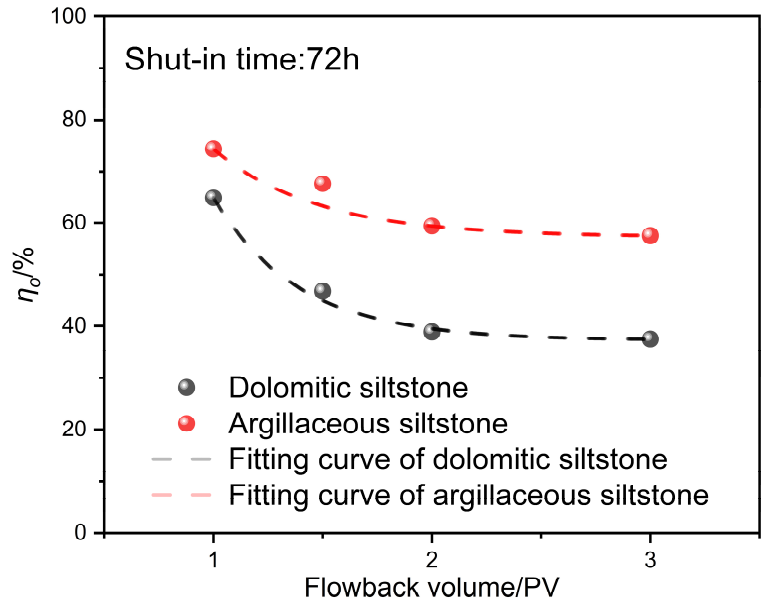

Figure 9. Permeability damage rate (η_o) versus flowback volume for Jimsar shale cores.

This rapid-then-slow recovery characteristic is closely related to the reservoir pore structure and multiphase flow mechanisms. During the initial flowback stage, the production differential pressure preferentially acts on the large pores and microfracture networks with the best flow capacity, where the retained fracturing fluid is efficiently displaced in a continuous phase. This stage is dominated by the cleanup of macroscopic flow channels, where each unit of flowback volume yields the most significant permeability recovery, corresponding to the steep decline segment of the damage rate-flowback volume curve. As flowback continues and free water in the large pores is essentially removed, the process enters a deep cleanup stage. The flow resistance at this stage mainly originates from two parts: first, the bound water trapped in micropores requires overcoming significant capillary pressure to initiate flow; second, dispersed droplets formed at some pore throats due to the Jamin effect require higher driving pressure to deform and pass through. These two parts collectively constitute the so-called "residual water block." The physical reason for this limit is governed by the capillary pressure, which is inversely proportional to the pore-throat radius. This defines a "Minimum Pore-Producing Radius" (MPPR) under a given drawdown pressure; fracturing fluid trapped in pores with throats smaller than this MPPR cannot be mobilized, permanently impairing the connected oil pathways. This leads to the flattening of the damage rate curve and exhibits an apparent recovery limit.

Notably, lithological differences also significantly affect the efficiency and limit of the flowback process. Owing to its relatively developed pore structure and weaker fluid-rock interactions, dolomitic siltstone approaches its recovery limit at a flowback volume of

2.0 PV, with a residual damage rate of about 38%, primarily attributable to liquid trapping in micropores and minimal chemical adsorption. In contrast, argillaceous siltstone not only suffers severe initial damage but also achieves a far inferior ultimate recovery compared to dolomitic siltstone, maintaining a damage rate of about 58% even at 3.0 PV flowback. This is mainly because, in addition to the ubiquitous water blocking effect, the inherently smaller and more tortuous pore structure of argillaceous siltstone means a larger proportion of its pore network falls below the MPPR. Furthermore, the migration of clay fines and partially irreversible hydration swelling generated during the fracturing fluid shut-in process cause permanent physical blockage of pore throats, effectively reducing the MPPR and further constricting flow pathways. This solid-phase damage cannot be remedied by fluid flowback.

Furthermore, the position of this economic critical point is not fixed but varies with lithology and operational practices. In dolomitic siltstone, the well-connected pore network allows for efficient cleanup, leading to an earlier plateau. In argillaceous siltstone, however, the stronger capillary trapping and potential for clay-induced damage necessitate a greater relative flowback volume to approach a (still lower) recovery limit. Operational factors, such as flowback rate and the use of surfactants to reduce interfacial tension, can also shift this critical point by altering the balance of viscous and capillary forces.

It is noteworthy that the pore volume (PV) referenced in this study is defined at the core-plug scale. In field operations, the total volume of fracturing fluid injected is substantially less than the total PV of the reservoir. Therefore, the critical value of ~2.0 PV identified in the experiments should be interpreted as a normalized parameter relative to the core PV, which primarily reveals the law of diminishing marginal returns in flowback efficiency, rather than a direct volumetric target for the field.

The practical implication for field operations is to prioritize the early-stage flowback phase. The experimental data indicate that the critical window for effective permeability recovery occurs within the initial flowback stage (corresponding to approximately 0.5–1.0 PV at the core scale). Translating this to the field, operators should focus on achieving an efficient initial flowback rate (e.g., the first 30–50% of the injected fluid volume) through optimized flowback strategies, such as controlled flowback rates and the application of cleanup additives. This approach maximizes the cleanup of the critical fracture-matrix network before the recovery efficiency plateaus.

3.4. Implications for Fracturing Operations

This study systematically reveals the microscopic mechanisms of fracturing fluid migration and damage in the Jimsar shale oil reservoir through NMR imbibition experiments and permeability damage evaluation, clarifying the intrinsic relationships among lithology, shut-in time, and flowback strategy. Based on the experimental results, the following comprehensive engineering recommendations are proposed to achieve the development goal of mitigating damage and enhancing production

First, fracturing design should fully account for the dominant role of reservoir lithology and implement tailored strategies. For dolomitic siltstone reservoirs, which have relatively developed pore structures and high imbibition displacement efficiency, the engineering focus should be on promoting imbibition by optimizing fracturing fluid volume and properties to maximize the utilization of their favorable spontaneous imbibition capability. For argillaceous siltstone reservoirs, characterized by high clay content, developed micropores, and high damage potential, the strategy must shift toward active protection. This necessitates enhancing the use of clay stabilizers and surfactants in the fracturing fluid to inhibit hydration swelling and water blocking, thereby controlling the extent of fracturing fluid invasion from the source.

Second, optimizing the shut-in schedule requires balancing the competing effects of imbibition displacement and reservoir damage. Experiments indicate a critical temporal window for the shut-in process; terminating it too early results in insufficient oil displacement, whereas an excessively long shut-in period aggravates liquid retention and physico-chemical damage. Field operations can make dynamic adjustments based on real-time data, such as formation pressure buildup dynamics, in conjunction with reservoir lithological characteristics. Generally, for damage-prone reservoirs like argillaceous siltstone, appropriately shortening the shut-in time should be considered, whereas for reservoirs with good imbibition capacity like dolomitic siltstone, the shut-in time can be extended to promote oil displacement.

Finally, the flowback strategy should prioritize efficiency and economic benefit. Although increasing the flowback volume helps restore permeability, its improvement effect exhibits significant diminishing marginal returns. An economic critical point for the flowback volume should be determined, with a focus on ensuring efficiency during the initial flowback stage to rapidly remove retained fluid from the main flow channels. Once permeability recovery plateaus in the later stages of flowback, indiscriminate pursuit of higher flow rates should be avoided to prevent unnecessary operational costs.

4. Conclusions

This study employed an integrated approach using NMR technology and core flooding experiments to systematically investigate the fracturing fluid imbibition characteristics and permeability damage mechanisms of two typical lithotypes (dolomitic siltstone and argillaceous siltstone) in the Jimsar shale oil reservoir. By combining dynamic 1D NMR profiling with standard T_2 spectrum analysis, the methodology provided insights beyond conventional T_2 analysis, uniquely capturing the spatiotemporal evolution of fracturing fluid invasion and the concomitant pore-scale fluid redistribution. The main conclusions are as follows:

(1) Reservoir lithology exerts a fundamental control on the imbibition behavior of fracturing fluid through its mineral composition and pore structure. Dolomitic siltstone, characterized by high brittle mineral content, developed intergranular pores, and superior pore connectivity, exhibits stronger spontaneous imbibition capacity and a greater fracturing fluid invasion depth (30.47 mm), resulting in higher oil displacement efficiency. In contrast, argillaceous siltstone, due to its high clay content and complex micropore system, promotes strong capillary trapping and potential physico-chemical damage, which severely restricts both fracturing fluid invasion (23.44 mm) and displacement efficiency.

(2) The degree of permeability damage induced by fracturing fluid retention exhibits significant lithological dependence. Argillaceous siltstone cores demonstrate a stronger damage potential, with a final permeability damage rate (η_o) (~70%) substantially higher than that of dolomitic siltstone (~46%). The damage mechanism in argillaceous siltstone is dominated by a compounded effect of "water blocking + clay hydration swelling/fine migration," whereas in dolomitic siltstone, it is primarily governed by a more manageable "water blocking" mechanism.

(3) The influence of shut-in time on the η_o follows a non-monotonic trend, revealing a dynamic competition between the detrimental effect of "fracturing fluid invasion damage" and the beneficial effect of "oil imbibition displacement." An optimal shut-in time window exists to maximize net benefits, and this window is lithology-dependent. For argillaceous siltstone reservoirs, caution is warranted against the risk of aggravated damage from excessively long shut-in times.

(4) The flowback strategy is critical for mitigating reservoir damage; however, its effectiveness is subject to a distinct economic marginal effect. Core-scale flowback experi-

ments reveal that the initial stage (corresponding to the first ~0.5–1.0 PV of fluid recovered) constitutes a "golden period" for permeability recovery, as it effectively cleans up the dominant flow channels. This finding, when translated to field operations, underscores the importance of optimizing early-flowback efficiency (e.g., recovering the initial 30–50% of the injected fluid volume) rather than pursuing total fluid recovery. Beyond this critical phase, permeability improvement becomes marginal because the residual damage stems primarily from fluids trapped in micropores and irreversible physical blockages that are impractical to remove.

Author Contributions: Conceptualization, L.B. and S.Z.; methodology, H.G.; validation, Z.J.; formal analysis, Y.S.; investigation, Y.L.; resources, Y.L.; data curation, Y.H.; writing—original draft preparation, H.G. and X.H.; writing—review and editing, L.B.; visualization, X.H.; supervision, S.Z.; project administration, S.Y. and S.Z.; funding acquisition, S.Y. All authors have read and agreed to the published version of the manuscript.

Funding: This research was funded in part by the National Natural Science Foundation of China, grant number 51574257, and the National Key Research and Development Program of China, grant number 2015CB250904.

Data Availability Statement: Data are available on request from the authors.

Acknowledgments: The authors would like to thank the National Fund Commission of China for providing financial support.

Conflicts of Interest: Authors Lei Bai, Huiying Guo, Zhaowen Jiang, Yating Sun, and Yan Li were employed by the Xinjiang Oilfield Company. The remaining authors declare that the research was conducted in the absence of any commercial or financial relationships that could be construed as a potential conflict of interest.

References

1. Zhang, L.; Pan, L.; Zou, Y.; Wang, J.; Li, M.; Feng, W. Recent Advances in Reservoir Stimulation and Enhanced Oil Recovery Technology in Unconventional Reservoirs. *Processes* **2024**, *12*, 10234. [CrossRef]
2. Chen, W.D.; Geng, X.F.; Liu, W.D.; Ding, B.; Xiong, C.M.; Sun, J.F.; Wang, C.; Jiang, K. A Comprehensive Review on Screening, Application, and Perspectives of Surfactant-Based Chemical-Enhanced Oil Recovery Methods in Unconventional Oil Reservoirs. *Energy Fuels* **2023**, *37*, 4729–4750. [CrossRef]
3. McMahon, T.P.; Larson, T.E.; Zhang, T.; Shuster, M. Geologic characteristics, exploration and production progress of shale oil and gas in the United States: An overview. *Pet. Explor. Dev.* **2024**, *51*, 925–948. [CrossRef]
4. Zhang, Z.M. Current Situation and Existing Problems of Horizontal Well Fracturing Technology. *Chem. Technol. Fuels Oils* **2024**, *60*, 1307–1312. [CrossRef]
5. Feng, R.Y.; Li, C.; Sun, L.C.; Wang, J.; Liu, J.; Li, N. Study on the Influence of Deep Coalbed Methane Horizontal Well Deployment Orientation on Production. *Energies* **2024**, *17*, 5784. [CrossRef]
6. Liu, R.H.; Sun, Y.; Wang, X.R.; Yan, B.Q.; Yu, L.M.; Li, Z. Production Capacity Variations of Horizontal Wells in Tight Reservoirs Controlled by the Structural Characteristics of Composite Sand Bodies: Fuyu Formation in the Qian'an Area of the Songliao Basin as an Example. *Processes* **2023**, *11*, 1824. [CrossRef]
7. Zhou, Z.; Abass, H.; Li, X.; Teklu, T. Experimental investigation of the effect of imbibition on shale permeability during hydraulic fracturing. *J. Nat. Gas. Sci. Eng.* **2016**, *29*, 413–430. [CrossRef]
8. Da, Q.; Yao, C.; Zhang, X.; Li, L.; Lei, G. Reservoir Damage Induced by Water-Based Fracturing Fluids in Tight Reservoirs: A Review of Formation Mechanisms and Treatment Methods. *Energy Fuels* **2024**, *38*, 18093–18115. [CrossRef]
9. Fu, L.; Liao, K.; Ge, J.; Huang, W.; Chen, L.; Sun, X.; Zhang, S. Study on the damage and control method of fracturing fluid to tight reservoir matrix. *J. Nat. Gas. Sci. Eng.* **2020**, *82*, 103464. [CrossRef]
10. Chen, Z.; Chen, J.; Zhang, X. A comprehensive review of minimum miscibility pressure determination and reduction strategies between CO_2 and crude oil in CCUS processes. *Fuel* **2025**, *384*, 134053. [CrossRef]
11. Guo, B.; Wortman, P. Understanding the post-frac soaking process in multi-fractured shale gas-oil wells. *Capillarity* **2024**, *12*, 6–16. [CrossRef]
12. Ibrahim, A.F.; Nasr-El-Din, H.A. Effect of well shut-in after fracturing operations on near wellbore permeability. *J. Pet. Sci. Eng.* **2019**, *181*, 106213. [CrossRef]

13. Hun, L.; Bing, Y.; Xixiang, S.; Xinyi, S.; Lifei, D. Fracturing fluid retention in shale gas reservoir from the perspective of pore size based on nuclear magnetic resonance. *J. Hydrol.* **2021**, *601*, 126590. [CrossRef]
14. Long, A.; Zhang, Y.; Zhao, Y.; Wu, S. Damage evolution characteristics caused by fluid infiltration across diverse injection rates: Insights from integrated NMR and hydraulic fracturing experiments. *J. Rock. Mech. Geotech. Eng.* **2025**, *17*, 5753–5767. [CrossRef]
15. Zhao, S.; Yang, S.-L.; Zuo, H.-W.; Liu, X.-Y.; Dang, Y.-L.; Zhang, Y.-Q.; Wang, B.-D.; Hu, J.-T.; Bai, H.-Y.; Han, Y.-N. NMR-Visualized Mechanisms of Nanoparticle-Stabilized Ternary CO_2 Foam for EOR in Low-Permeability Reservoirs. *Energy Fuels* **2025**, *39*, 21412–21421. [CrossRef]
16. Zhao, S.; Yang, S.-L.; Bai, H.-Y.; Han, Y.-N.; Wang, B.-D.; Yang, K.; Hu, J.-T.; Luo, Y.; Liu, X.-Y. Enhancing oil recovery in tight fractured reservoirs: An NMR study of foam flooding with imbibition effects. *Colloids Surf. A Physicochem. Eng. Asp.* **2025**, *726*, 137745. [CrossRef]
17. Guo, H.; Wang, Z.; Zhang, Y.; Sun, Y.; Liu, S.; Li, Z.; Liu, Y.; Yang, S.; Zhao, S. Influence of Shale Mineral Composition and Proppant Filling Patterns on Stress Sensitivity in Shale Reservoirs. *Processes* **2024**, *12*, 789. [CrossRef]
18. Chen, H.; Chen, Z.; Wei, B.; Jiang, Q. A novel approach for quantitative characterization of aqueous in-situ foam dynamic structure based on fractal theory. *Fuel* **2023**, *352*, 129149. [CrossRef]
19. Rezaeizadeh, M.; Hajiabadi, S.H.; Aghaei, H.; Blunt, M.J. Pore-scale analysis of formation damage; A review of existing digital and analytical approaches. *Adv. Colloid. Interface Sci.* **2021**, *288*, 102345. [CrossRef] [PubMed]
20. Minh, C.C.; Jaffuel, F.; Poirier, Y.; Haq, S.A.; Baig, M.H.; Jacob, C. Quantitative Estimation Of Formation Damage From Multi-Depth Of Investigation Nmr Logs. In Proceedings of the SPWLA 52nd Annual Logging Symposium, Colorado Springs, CO, USA, 14–18 May 2011.

Disclaimer/Publisher's Note: The statements, opinions and data contained in all publications are solely those of the individual author(s) and contributor(s) and not of MDPI and/or the editor(s). MDPI and/or the editor(s) disclaim responsibility for any injury to people or property resulting from any ideas, methods, instructions or products referred to in the content.